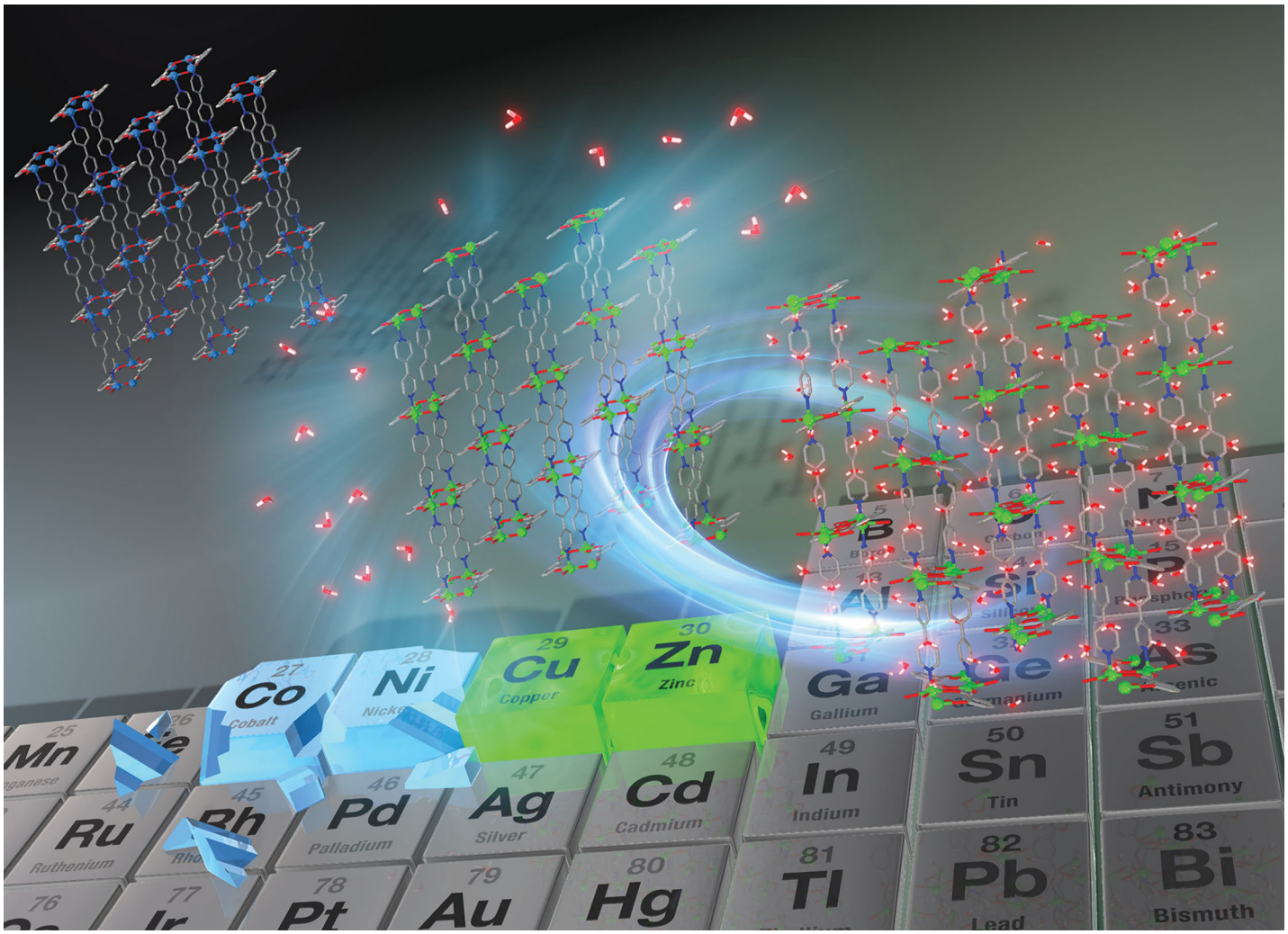

Showcasing research from Professor Tanaka's laboratory, Department of Chemistry, School of Science and Technology, Kwansei Gakuin University, 2-1 Gakuen, Sanda, Hyogo 669-1337, Japan.

Coordination distortion induced water adsorption in hydrophobic flexible metal–organic frameworks

We synthesized four isostructural flexible interdigitated hydrophobic metal–organic frameworks that differ only in their central metal ion. The water-adsorption properties are dependent on the metal species, which was revealed to be caused by coordination distortion around the metal ions.

As featured in:

See Daisuke Tanaka *et al.*, *Chem. Commun.*, 2020, **56**, 9106.

ROYAL SOCIETY OF CHEMISTRY

rsc.li/chemcomm

Registered charity number: 207890

ChemComm

ROYAL SOCIETY OF CHEMISTRY

COMMUNICATION

View Article Online
View Journal | View Issue

Cite this: *Chem. Commun.*, 2020, **56**, 9106

Received 28th May 2020,
Accepted 16th July 2020

DOI: 10.1039/d0cc03772a

rsc.li/chemcomm

Coordination distortion induced water adsorption in hydrophobic flexible metal–organic frameworks†

Yoshinobu Kamakura,[a] Arata Hikawa,[a] Hirofumi Yoshikawa,[b] Wataru Kosaka,[cd] Hitoshi Miyasaka[cd] and Daisuke Tanaka*[ae]

Herein, we synthesized four isostructural flexible interdigitated hydrophobic metal–organic frameworks that differ only in their central metal ion. The water-adsorption properties are dependent on the metal species, which was revealed to be caused by coordination distortion around the metal ions.

Recently, metal–organic frameworks (MOFs) have attracted significant attention for use as water adsorbents.[1–5] MOFs exhibit several attractive properties, which make them suitable for use in several applications, including fluorescence,[6–8] phosphorescence,[9,10] enhanced CO_2 capture,[11,12] ion conduction,[13,14] and dehumidification.[15,16] The ability to adsorb and desorb water molecules at high relative pressures can help in reducing the amount of energy consumed during the release of water. Therefore, flexible[17–19] and mesoporous[20–22] MOFs have been developed. Flexible MOFs are particularly desirable as they facilitate fine control of the onset pressure; they exhibit abrupt uptake at a specific pressure, which is referred to as the gate-opening pressure.[23] This onset pressure is significantly affected by the flexibility of the linker,[24] structural dimensionality,[25] and type of metal ion used in the nodes.[26]

To control the onset pressure for the adsorption of water molecules by a flexible MOF, the relationship between the framework dynamics and behavior of the water molecules in the micropores of the MOF must be known. In particular, flexible MOFs with low structural dimensionality and coordination distortion within their nodes are interesting because their onset pressure is affected by various structural parameters. In this work, we chose MCID-1 ($[M(ip)(bpy)]_n$, where M = metal ion, ip = isophthalate, and bpy = 4,4′-bipyridine) as the model compound. The metal ions in MCID-1 are connected by ip units to form one-dimensional (1D) double-chain ribbon-like structures of $\{[M(ip)]\}_n$. Then, these ribbons are linked by bpy to yield a two-dimensional (2D) sheet-like motif. Finally, these 2D layers are mutually interdigitated, resulting in zero-dimensional (0D) hydrophobic pores between the layers (Fig. 1a).[27] MCID-1 adsorbs guest molecules, which is accompanied by the expansion of the 2D layer gap and rearrangement of the coordination modes of the metal ions. In addition, MCID-1 forms isostructures with various metal ions.[28–33] Although these characteristics are desirable for evaluating the effects of node-derived flexibility

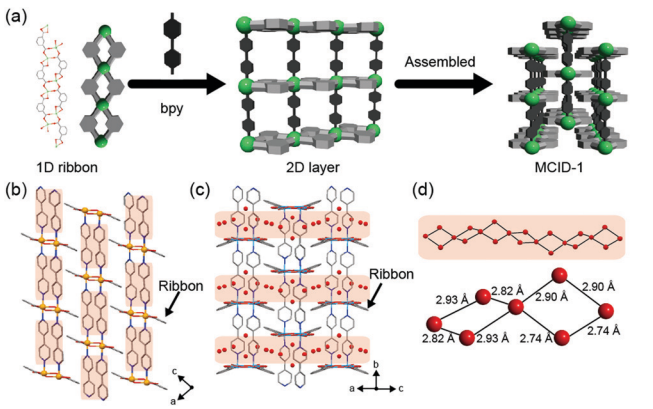

Fig. 1 (a) MCID-1 assembly process. Crystal structures of (b) CoCID-1, (c) CuCID-1⊃H_2O, and (d) CuCID-1. The pale-red highlighted regions in (b) and (c) represent pore spaces. The pale-red highlighted region in (c) represents the water chain structure in the 1D channel. Orange, gray, blue, and red represent Co, C, N, and O, respectively. H atoms are omitted for clarity.

[a] *Department of Chemistry, School of Science and Technology, Kwansei Gakuin University, 2-1 Gakuen, Sanda, Hyogo 669-1337, Japan. E-mail: dtanaka@kwansei.ac.jp*
[b] *Department of Nanotechnology for Sustainable Energy, School of Science and Technology, Kwansei Gakuin University, Sanda, Hyogo 669-1337, Japan*
[c] *Institute for Materials Research, Tohoku University, 2-1-1 Katahira, Aoba-ku, Sendai 980-8577, Japan*
[d] *Department of Chemistry, Graduate School of Science, Tohoku University, 6-3 Aramaki-Aza-Aoba, Aoba-ku, Sendai 980-8578, Japan*
[e] *JST PRESTO, 2-1 Gakuen, Sanda, Hyogo 669-1337, Japan*

† Electronic supplementary information (ESI) available: Experimental information, structural figures and tables, additional data. CCDC 1978140. For ESI and crystallographic data in CIF or other electronic format see DOI: 10.1039/d0cc03772a

and dimensionality, apart from ZnCID-1, the water-adsorption properties of MCID-1 compounds have not yet been reported. Therefore, the effect of the type of metal ion on the water-adsorption behavior of these compounds remains unknown. Herein, we report the effects of various central metal species on the water-adsorption behavior of MCID-1 and highlight the differences in these behaviors for four MCID-1 compounds (M = Co, Ni, Cu, and Zn). Moreover, we synthesized solid-solution-type M1M2CID-1 and determined the correlation between the distribution of metal ions within the framework and its water-adsorption behavior.

MCID-1 was synthesized by the solvothermal method through the reaction of $M(NO_3)_2{\cdot}xH_2O$ (M = Co, Ni, and Zn, x = 6 or M = Cu, x = 3) with Na_2ip and bpy (M : Na_2ip : bpy molar ratio = 1 : 1 : 1) in H_2O with heating at 150 °C for 48 h followed by cooling to 30 °C over 12 h. We obtained MCID-1 in powdered form under various synthesis conditions. The X-ray powder diffraction (XRPD) patterns of the synthesized samples are identical to those simulated based on the reported crystal structure of MCID-1 (Fig. S1, ESI†). The XRPD patterns of the as-synthesized CoCID-1 and NiCID-1 are identical to those of the guest-free phase, which indicates that both compounds are devoid of guest water molecules in their 0D hydrophobic cavities (Fig. 1b and Fig. S2a; see note S5 in the ESI†).[30,31] However, the XRPD patterns of CuCID-1 and ZnCID-1 indicate the presence of water molecules within the pores (MCID-1⊃H_2O; Fig. 1c and Fig. S2e; see note S5 in the ESI†), although the areas surrounding the pores in MCID-1 are hydrophobic (Fig. 1c and Fig. S2d, ESI†).[32,33] The XRPD patterns of MCID-1⊃H_2O (M = Cu or Zn) indicate ribbon-like structures, *i.e.*, structures in which the aromatic rings in the coordination polymer of metal ions and ip are twisted alternately. The twisted ribbon-like structures result in the formation of 1D channels. These 1D channels are filled with water molecules, which form 1D chain structures within the hydrophobic space due to hydrogen bonding.[34] The formation of water nanoclusters plays a key role in stabilizing these 1D chain structures (Fig. 1c and d).

Guest-free MCID-1 was obtained by washing MCID-1 with MeOH and heating it at 120 °C overnight under reduced pressure. The XRPD patterns of CoCID-1 and NiCID-1 did not change during degassing/activation (Fig. S4 and S5, ESI†). In contrast, the XRPD patterns of CuCID-1⊃H_2O and ZnCID-1⊃H_2O changed upon removal of water. The XRPD pattern of ZnCID-1⊃H_2O after degassing is identical to the simulated pattern of degassed ZnCID-1 (Fig. S6, ESI†), whose space group is similar to that of CoCID-1 and NiCID-1 ($P\bar{1}$).[33] In contrast, the XRPD pattern of CuCID-1 acquired in an Ar atmosphere is dramatically different from that of MCID-1⊃H_2O and corresponds to an unknown phase (Fig. S7 and S8, ESI†). We successfully determined the crystal structure of the guest-free CuCID-1 phase through single-crystal structural analysis (Fig. 1c and Table S1, ESI†). While the other MCID-1 samples (M = Co, Ni, and Zn) had a space group of $P\bar{1}$, that of CuCID-1 was determined to be $P2_1/c$ (Table S2, ESI†). The simulated XRPD pattern of the degassed CuCID-1 phase is identical to this unknown XRPD pattern. CuCID-1 adsorbed water in air, and its crystal structure transformed to that of CuCID-1⊃H_2O within 20 min under ambient conditions (Fig. S8, ESI†).

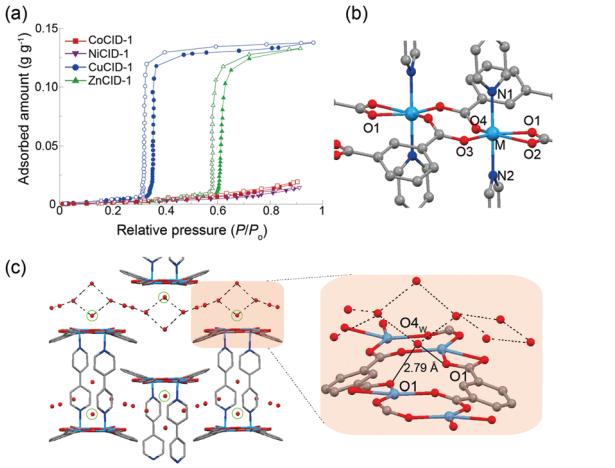

Fig. 2 (a) Adsorption and desorption isotherms for water at 298 K. Filled and open symbols correspond to adsorption and desorption, respectively. Coordination structure of CuCID-1⊃H_2O around (b) metal ion and (c) $O4_w$.

To evaluate the affinity of MCID-1 for water, the water-adsorption isotherms of MCID-1 were acquired, which showed that the onset pressure (P/P_0) for ZnCID-1 was approximately 0.60 and similar to that reported previously,[27] while CuCID-1 started to adsorb water at approximately P/P_0 = 0.33 (Fig. 2a). In contrast, CoCID-1 and NiCID-1 did not adsorb water below P/P_0 = 0.9. These results indicate that the adsorption behavior of MCID-1 changed considerably, although the hydrophobic cavity environment remained similar (see note S10 in the ESI†) and the metal ions and water molecules do not directly interact.

To understand the differences in these water-adsorption properties, we focused on the coordination environment of MCID-1 (Table S2, ESI†). The nodes of MCID-1 are dinuclear complexes, wherein the two metal ions are crystallographically equivalent and exhibit six-fold coordination structures (Fig. 2b and Fig. S10a, ESI†). The lengths of the six coordination bonds in CoCID-1 and NiCID-1 are almost the same (2.0–2.2 Å). Furthermore, the coordination geometries of CoCID-1 and NiCID-1 are similar to that of a symmetric ideal octahedron. However, for CuCID-1⊃H_2O and ZnCID-1⊃H_2O, the length of the bond between the metal atom and one of the oxygen atoms (M–O2) is approximately 2.6 Å, which is approximately 0.5 Å longer than that of the other bonds. In other words, the metal ion in MCID-1⊃H_2O exhibits a distorted octahedral geometry. In the case of degassed ZnCID-1, the coordination distortion relaxes once the water molecules are removed. The space group of ZnCID-1 changes from $C2/c$ to $P\bar{1}$, which is similar to that of CoCID-1 and NiCID-1. However, the Cu–O2 bond length does not change after the removal of the guest, and CuCID-1 still shows coordination distortion, which is attributable to the Jahn–Teller effect of Cu^{II}. In addition, the space group of CuCID-1 is $P2_1/c$, which is different from that of the other degassed MCID-1 phases. These results suggest that the adsorption of water induces distortion of the coordination structure

and the stability of the distorted coordination structure depends on the type of metal ion used.

In contrast, the crystal structure of MCID-1⊃H_2O suggests that the guest water molecules form 1D chains through hydrogen-bonding interactions within the pores. In addition, one of the water molecules ($O4_w$) in the 1D chain forms a hydrogen bond with the oxygen atom of the carboxylate of ip (O1) (Fig. 2c and Fig. S10b, ESI†). It is likely that this host–guest interaction leads to coordination distortion, resulting in the structural transition. These results suggest that the coordination structure around the metal ion requires this distortion to interact with $O4_w$, after which the coordination bond length of M–O2 increases. In other words, the distortion of the coordination bond is important for the formation of the hydrogen bond between O1 and $O4_w$. Furthermore, it is likely that the differences in stabilities of the distorted structures corresponding to the various metal ions determine the water-adsorption properties of MCID-1.

We propose an energy diagram to explain the metal-ion dependency of the water-adsorption behavior of MCID-1 (Fig. 3). We hypothesize that MCID-1 exhibits the following three phases: a closed phase (CP), imaginary open phase without water molecules (OP), and open phase with water (OP⊃H_2O). In addition, two types of variations in energy are defined: one is the change in the Gibbs energy for structural transformation (ΔG_{ST}), which destabilizes OP⊃H_2O, whereas the other is the change in the Gibbs energy for water-cluster formation (ΔG_{water}), which stabilizes OP⊃H_2O. Initially, we assumed that the CP structure of the $P\bar{1}$ group of MCID-1 (M = Co, Ni, and Zn) and the CP structure of the $P2_1/c$ group of CuCID-1 have the same Gibbs energies. Focusing on the value of ΔG_{ST}, for this assumption to be true, the coordination bonds must lengthen and coordination structure must distort. We believe that the ΔG_{ST} value of CuCID-1 is the smallest because the distorted coordination structure of Cu^{II} is stable even in the absence of guest molecules, owing to the Jahn–Teller effect. In contrast, since the symmetric coordination structures of NiCID-1 and CoCID-1 do not contain water molecules, their ΔG_{ST} values are expected to be very large, which is mostly due to the absence of the Jahn–Teller effect. Furthermore, the ΔG_{ST} value of ZnCID-1 is expected to be moderately high and the distorted coordination structure is somewhat stable because of the isotropic d^{10} electron structure of Zn^{II} ion. In addition, we assume that similar water chain structures are formed in all MCID-1 samples. Therefore, their ΔG_{water} values are also the same. As shown in Fig. 3, CuCID-1 and ZnCID-1 are stabilized by the water chain, and the as-synthesized compounds are MCID-1⊃H_2O (M = Cu, and Zn). Furthermore, this model suggests that CuCID-1⊃H_2O is more stable than ZnCID-1⊃H_2O, which is consistent with the lower onset pressure observed in the CuCID-1 water-adsorption isotherm. However, CoCID-1 and NiCID-1 are destabilized after water adsorption, as their ΔG_{ST} values are high. Thus, they cannot form OP⊃H_2O due to this type of destabilization. The proposed energy diagram strongly suggests that coordination distortion is essential for the adsorption of water into the pores. Furthermore, the onset pressure depends on the stability of the distorted coordination structure, and distortion is accompanied by a structural transformation. Therefore, the adsorption behavior of MCID-1 is strongly affected by the type of central metal ion present.

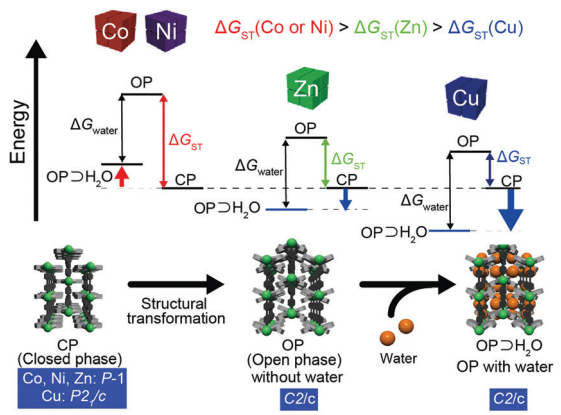

Fig. 3 Proposed energy diagram for the structural transformation. If the ΔG_{ST} values for CoCID-1 and NiCID-1 are much larger than proposed, OP⊃H_2O for CoCID-1 and NiCID-1 will be more unstable than OP for ZnCID-1 and CuCID-1, which cannot be confirmed from the experimental results.

The metal-based solid solution approach is a recently developed method for precisely controlling the flexibility of a MOF.[35] With the aim of controlling the adsorption behavior of MCID-1, we evaluated the adsorption behavior of solid-solution-type CID-1 ($M1_xM2_{1-x}$CID-1). We synthesized solid-solution-type $M1_xM2_{1-x}$CID-1 with various metal ratios under the same synthesis conditions as those used to prepare MCID-1, with the only difference being the ratio of M1 and M2 (M1 : M2 : Na_2ip : bpy = x : 1 − x : 1 : 1; x = 0.15, 0.33, 0.50, 0.67, and 0.85). The XRPD patterns and scanning electron microscopy-energy-dispersive X-ray spectroscopy (SEM-EDX) maps show that Cu-containing CID-1 (Cu_xM_{1-x}CID-1) does not form a uniform solid-solution-type CID-1 at any metal ratio. However, other metal combinations yielded well-mixed $M1_xM2_{1-x}$CID-1 (Fig. 4a; also see notes S12–S15 in the ESI†). To evaluate the distribution structures, we measured their magnetic susceptibilities.[36] The results suggest that $M_{0.5}Zn_{0.5}$CID-1 (M = Co and Ni) forms homo-metal dinuclear structures. However, $Co_{0.5}Ni_{0.5}$CID-1 exhibited a randomly mixed hetero- and homo-metal dinuclear structure (see note S16 in the ESI†).

Next, we acquired the water-sorption isotherms of $M1_xM2_{1-x}$CID-1 at 298 K to evaluate the effects of the type of metal ion in the solid solution, which revealed that the onset pressure changes gradually with metal-ion ratio (see note S17 in the ESI†). The isotherms for Zn_xM_{1-x}CID-1 (M = Co and Ni) suggest that the amount of water adsorption increases gradually with increasing x, while the isotherms for Cu_xM_{1-x}CID-1 (M = Co, Ni, and Zn) indicate stepwise adsorption, *i.e.*, the adsorption has two components, which is consistent with the heterogeneous distribution of Cu ions observed in the SEM-EDX map in Fig. 4a. These results suggest that the onset pressure and adsorption amount can be controlled by mixing the metal ions. With respect to the amount of water adsorbed by $M1_{0.5}M2_{0.5}$CID-1 (Fig. 4b), the amount of

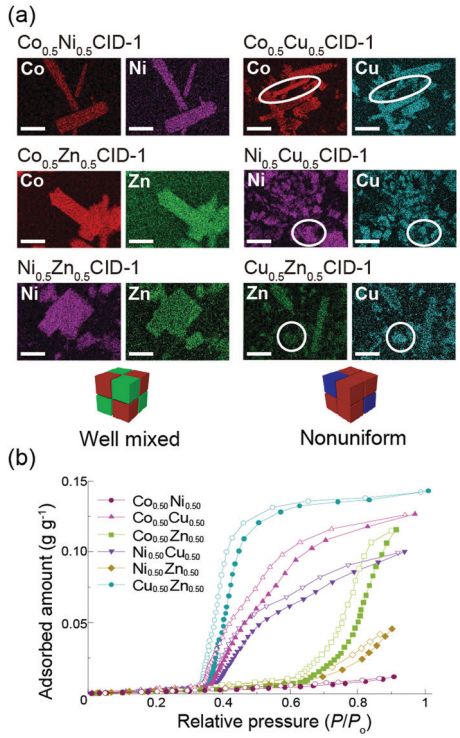

Fig. 4 (a) SEM-EDX maps for $M1_{0.5}M2_{0.5}$CID-1. White circles indicate nonuniform areas. Scale bars: 30 μm. (b) Water-sorption isotherms of $M1_{0.5}M2_{0.5}$CID-1 at 298 K. Filled and open symbols correspond to adsorption and desorption, respectively.

adsorbed water by $Co_{0.5}Zn_{0.5}$CID-1 was larger than that of $Ni_{0.5}Zn_{0.5}$CID-1, which is attributable to the weak Jahn–Teller effect of the Co^{II} (d^7) metal ion, which aids distortion and structural transformation as a consequence.

In summary, we demonstrated that the water-adsorption behavior of MCID-1 (M = Co, Ni, Cu, and Zn) strongly depends on the type of metal ion. The formation of 1D water chain-like structures is the key factor that determines the adsorption of water within the hydrophobic pores. In addition, Jahn–Teller stabilization of the distorted coordination structure enables water adsorption at lower pressures. Further, the adsorbed amount and uptake pressure of water are determined by the composition of the M1M2CID-1 solid solution. This study provides a new strategy for controlling the water-adsorption properties of MOFs based on their design.

D. T. acknowledges the PRESTO program (Grant No. JPMJPR17NA) of the Japan Science and Technology Agency (JST) and the JSPS for KAKENHI Grant No. 20H02577. H. Y. acknowledges the JSPS for KAKENHI Grant No. 20H04680, 20H04646, and 18H04528. This work was performed under the GIMRT program of the Institute for Materials Research, Tohoku University (Proposal No. 18K0063). We thank Prof. R. Matsuda for his helpful discussion.

Conflicts of interest

There are no conflicts to declare.

References

1 M. J. Kalmutzki, C. S. Diercks and O. M. Yaghi, *Adv. Mater.*, 2018, **30**, e1704304.
2 J. Canivet, A. Fateeva, Y. Guo, B. Coasne and D. Farrusseng, *Chem. Soc. Rev.*, 2014, **43**, 5594.
3 Z. Chen, P. Li, X. Zhang, P. Li, M. C. Wasson, T. Islamoglu, J. F. Stoddart and O. K. Farha, *J. Am. Chem. Soc.*, 2019, **141**, 2900.
4 C. Wang, X. Liu, N. Keser Demir, J. P. Chen and K. Li, *Chem. Soc. Rev.*, 2016, **45**, 5107.
5 H. Kim, S. Yang, S. R. Rao, S. Narayanan, E. A. Kapustin, H. Furukawa, A. S. Umans, O. M. Yaghi and E. N. Wang, *Science*, 2017, **356**, 430.
6 X. Yang and D. Yan, *J. Mater. Chem. C*, 2017, **5**, 7898.
7 D. Yan, Y. Tang, H. Lin and D. Wang, *Sci. Rep.*, 2014, **4**, 4337.
8 X. Yang and D. Yan, *Chem. Sci.*, 2016, **7**, 4519.
9 X. Yang and D. Yan, *Adv. Opt. Mater.*, 2016, **4**, 897.
10 Y. Yang, K.-Z. Wang and D. Yan, *ACS Appl. Mater. Interfaces*, 2016, **8**, 15849.
11 E. Soubeyrand-Lenoir, C. Vagner, J. W. Yoon, P. Bazin, F. Ragon, Y. K. Hwang, C. Serre, J. S. Chang and P. L. Llewellyn, *J. Am. Chem. Soc.*, 2012, **134**, 10174.
12 A. O. Yazaydin, A. I. Benin, S. A. Faheem, P. Jakubczak, J. J. Low, R. R. Willis and R. Q. Snurr, *Chem. Mater.*, 2009, **21**, 1425.
13 S. S. Nagarkar, S. M. Unni, A. Sharma, S. Kurungot and S. K. Ghosh, *Angew. Chem., Int. Ed.*, 2014, **53**, 2638.
14 J. M. Taylor, K. W. Dawson and G. K. Shimizu, *J. Am. Chem. Soc.*, 2013, **135**, 1193.
15 R. G. AbdulHalim, P. M. Bhatt, Y. Belmabkhout, A. Shkurenko, K. Adil, L. J. Barbour and M. Eddaoudi, *J. Am. Chem. Soc.*, 2017, **139**, 10715.
16 P. Guo, A. G. Wong-Foy and A. J. Matzger, *Langmuir*, 2014, **30**, 1921.
17 A. Schneemann, V. Bon, I. Schwedler, I. Senkovska, S. Kaskel and R. A. Fischer, *Chem. Soc. Rev.*, 2014, **43**, 6062.
18 S. Horike, S. Shimomura and S. Kitagawa, *Nat. Chem.*, 2009, **1**, 695.
19 G. Ferey and C. Serre, *Chem. Soc. Rev.*, 2009, **38**, 1380.
20 A. Samokhvalov, *Chem. – Eur. J.*, 2015, **21**, 16726.
21 W. Xuan, C. Zhu, Y. Liu and Y. Cui, *Chem. Soc. Rev.*, 2012, **41**, 1677.
22 P. Silva, S. M. Vilela, J. P. Tome and F. A. Almeida Paz, *Chem. Soc. Rev.*, 2015, **44**, 6774.
23 D. Tanaka, K. Nakagawa, M. Higuchi, S. Horike, Y. Kubota, T. C. Kobayashi, M. Takata and S. Kitagawa, *Angew. Chem., Int. Ed.*, 2008, **47**, 3914.
24 A. X. Zhu, Q. Y. Yang, S. Mukherjee, A. Kumar, C. H. Deng, A. A. Bezrukov, M. Shivanna and M. J. Zaworotko, *Angew. Chem. Int. Ed.*, 2019, **58**, 18212.
25 A. Kondo, H. Kajiro, H. Noguchi, L. Carlucci, D. M. Proserpio, G. Ciani, K. Kato, M. Takata, H. Seki, M. Sakamoto, Y. Hattori, F. Okino, K. Maeda, T. Ohba, K. Kaneko and H. Kanoh, *J. Am. Chem. Soc.*, 2011, **133**, 10512.
26 J. Canivet, J. Bonnefoy, C. Daniel, A. Legrand, B. Coasne and D. Farrusseng, *New J. Chem.*, 2014, **38**, 3102.
27 S. Horike, D. Tanaka, K. Nakagawa and S. Kitagawa, *Chem. Commun.*, 2007, 3395.
28 S. Horike, M. Sugimoto, K. Kongpatpanich, Y. Hijikata, M. Inukai, D. Umeyama, S. Kitao, M. Seto and S. Kitagawa, *J. Mater. Chem. A*, 2013, **1**, 3675.
29 C. Ma, C. Chen, Q. Liu, D. Liao, L. Li and L. Sun, *New J. Chem.*, 2003, **27**, 890.
30 L.-F. Song, C.-H. Jiang, C.-L. Jiao, J. Zhang, L.-X. Sun, F. Xu, W.-S. You, Z.-G. Wang and J.-J. Zhao, *Cryst. Growth Des.*, 2010, **10**, 5020.
31 J. Tao, X.-M. Chen, R.-B. Huang and L.-S. Zheng, *J. Solid State Chem.*, 2003, **170**, 130.
32 Y.-H. Wen, J.-K. Cheng, Y.-L. Feng, J. Zhang, Z.-J. Li and Y.-G. Yao, *Inorg. Chim. Acta*, 2005, **358**, 3347.
33 Y. Kamakura, N. Hosono, A. Terashima, S. Kitagawa, H. Yoshikawa and D. Tanaka, *ChemPhysChem*, 2018, **19**, 2134.
34 T. Ohba, H. Kanoh and K. Kaneko, *J. Am. Chem. Soc.*, 2004, **126**, 1560.
35 J. Zhang, W. Kosaka and H. Miyasaka, *Chem. Lett.*, 2019, **48**, 1308.
36 G. Mali, M. Mazaj, I. Arcon, D. Hanzel, D. Arcon and Z. Jaglicic, *J. Phys. Chem. Lett.*, 2019, **10**, 1464.